Something something something physics

Steven Green
of Emmanuel College

Abstract

LHCb is a b-physics detector experiment which will take data at the
14 TeV LHC accelerator at CERN from 2007 onward...

Declaration

This dissertation is the result of my own work, except where explicit reference is made to the work of others, and has not been submitted for another qualification to this or any other university. This dissertation does not exceed the word limit for the respective Degree Committee.

Andy Buckley

Acknowledgements

Of the many people who deserve thanks, some are particularly prominent, such as my supervisor. . .

Preface

This thesis describes my research on various aspects of the LHCb particle physics program, centred around the LHCb detector and LHC accelerator at CERN in Geneva.

For this example, I'll just mention Chapter **??** and Chapter **??**.

x

Contents

"Writing in English is the most ingenious torture ever devised for sins committed in previous lives."
   — James Joyce

Chapter 1.

The Sensitivity of CLIC to Anomalous Gauge Couplings through Vector Boson Scattering

"Kids, you tried your best, and you failed miserably. The lesson is, never try."

— Homer Simpson

1.1. Background

A process that will show sensitivity to the α_4 and α_5 anomalous gauge couplings in the CLIC experiment is vector boson scattering. There are several channels that will be affected by these anomalous couplings at CLIC and these are summarised in figures **??**, **??**, reffig:vbswz and **??** where $q = $ u, d, s, b, c and $l = $ e, μ, τ, ν_e, ν_ν, ν_τ.

To determine whether an event is sensitive to α_4 and α_5 it will be necessary to determine whether the visible final states have been produced from the decay of W and Z bosons. A key discriminator in this procedure will be the invariant mass of the W and Z candidates. In light of this the hadronic decays of the W and Z bosons are only considered as the leptonic decays may contain neutrinos.

As the W and Z bosons in vector boson scattering are intermediate states in the Feynman diagrams, they will not be directly observed in the detector and will instead

contribute to processes with the final states containing possible decay products of the bosons $\nu\nu$qqqq, lνqqqq and llqqqq. In theory all processes will be affected by non zero α_4 and α_5, however, the effects may be extremely small as they contribute to very high order expansions of the Hamiltonian. Event generation software does not calculate the expansions of the Hamiltonian to all orders, but instead truncates the expansion to leave the dominant terms. In the case of anomalous couplings this corresponds to certain final state cross sections being invariant to changes in α_4 and α_5.

1.2. Event Generation

The event generation software used by the CLIC experiment is Whizard [7, 11]. Whizard version 1.97 was used for generating the new samples, while version 1.95 is used for the official CLIC samples. It was recommended by the Whizard authors to use version 1.97 as it contains a unitarisation scheme that ensures the probabilities remain physical up to high energies when considering the effect of anomalous gauge couplings.

It was necessary to specify the anomalous coupling model in Whizard to study their impact, however, this did enforce a unit CKM matrix. In the context of vector boson scattering this will restrict the decays of the W to d$\bar{\text{u}}$ and s$\bar{\text{c}}$, the W+ to u$\bar{\text{d}}$ and c$\bar{\text{s}}$ and the Z to u$\bar{\text{u}}$, d$\bar{\text{d}}$, s$\bar{\text{s}}$, c$\bar{\text{c}}$, b$\bar{\text{b}}$. This has little overall impact on the study as the cross section calculation using this model was, within the errors quoted by Whizard, identical to the standard model CKM matrix. The only aspect of the analysis affected by this modification is the flavour tagging of jets, however, this procedure while applied in this analysis is not used for event selection as it was found to be of negligible use in separating signal from background in subsequent chapter.

To find out which states show sensitivity to the anomalous couplings cross section calculations were made using different values of α_4 and α_5 for relevant processes involving the hadronic decays of the W and Z bosons from vector boson scattering. These results can be found in table 1.1 for 1.4 TeV samples and 1.2 for 3 TeV samples. The only final states showing sensitivity to the anomalous couplings are $\nu\nu$qqqq, lνqqqq and llqqqq, which correspond to the final states from the Feynman diagrams shown above in figures **??**, **??**, reffig:vbswz and **??**. As this analysis focuses on the hadronic decays of the bosons involved in vector boson scattering the final states involving leptonic decays of the bosons e.g. $\nu\nu$llqq were not included in this cross

check. These leptonic dominated final states were also removed from the background samples used in this study as isolated lepton finding would largely veto all such events from selection.

This cross check was also applied to the background samples that are to be included in this analysis. It was found that the cross sections was invariant to changes in α_4 and α_5 for the following processes:

- $e^+e^- \to qqqq$

- $e^+e^- \to \nu\nu qq$

- $e^+e^- \to l\nu qq$

- $e^+e^- \to llqq$

- $e^+e^- \to qq$

- $\gamma_{EPA}e^- \to qqqqe^-$

- $\gamma_{BS}e^- \to qqqqe^-$

- $e^+\gamma_{EPA} \to qqqqe^+$

- $e^+\gamma_{BS} \to qqqqe^+$

- $\gamma_{EPA}e^- \to qqqq\nu$

- $\gamma_{BS}e^- \to qqqq\nu$

- $e^+\gamma_{EPA} \to qqqq\nu$

- $e^+\gamma_{BS} \to qqqq\nu$

- $\gamma_{EPA}\gamma_{EPA} \to qqqq$

- $\gamma_{EPA}\gamma_{BS} \to qqqq$

- $\gamma_{BS}\gamma_{EPA} \to qqqq$

- $\gamma_{BS}\gamma_{BS} \to qqqq$

The sensitivity of an individual event to the anomalous gauge couplings is determined through an event weight. This weight corresponds to the ratio using non-zero α_4 and α_5 and using zero α_4 and α_5 of the square of the matrix element used in the cross section calculation. This reweighting procedure has many advantages over the
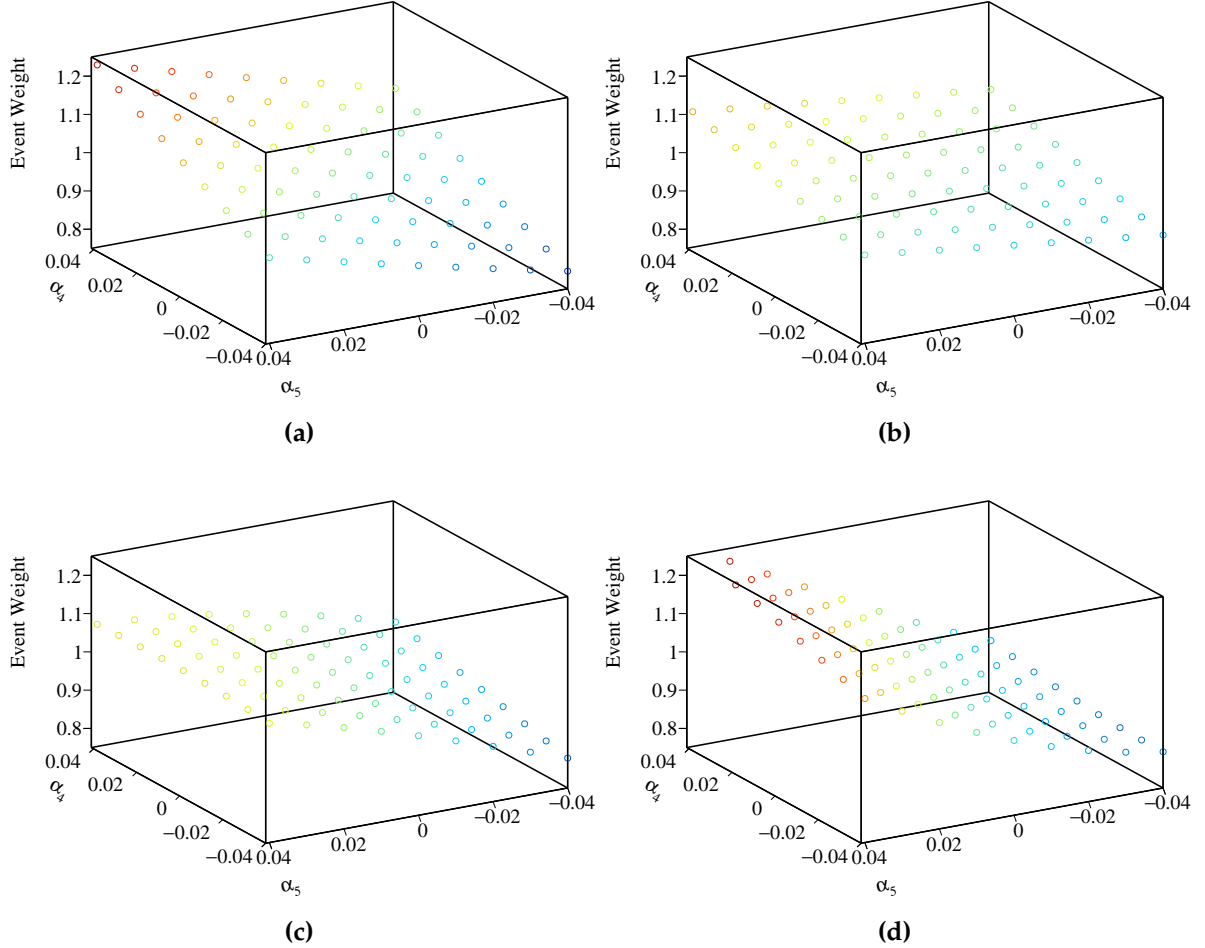
Figure 1.1.: A selection of plots showing how the event weight changes when varying the anomalous couplings α_4 and α_5 for 1.4TeV $\nu\nu$qqqq final state events.

alternative procedure of generating new samples with fixed α_4 and α_5 most notably the absence of systematic errors that may appear in new event generation. Each event picks up different weights based on α_4 and α_5 as the matrix element contributions from the anomalous couplings depend upon the kinematics of the final state, which is unique for each event. Examples of the event weights as a function of α_4 and α_5 for selected events is shown in figure 1.4.

The cross check shows that the most sensitive channel to the anomalous gauge couplings is the $\nu\nu$qqqq indicating that the best sensitivity measurement should focus upon this channel, which is the aim of this analysis.

The CLIC experiment has a repository of simulated and reconstructed samples that can be used for physics analyses, however, for the relevant final states there is

no way to calculate the event weights for these samples. Therefore, new samples for which reweighting is possible were created and processed through the CLIC reconstruction chain. New samples were created only for the $\nu\nu$qqqq final state as the lνqqqq and llqqqq final states have a significantly lower sensitivity. As will be shown in subsequent chapters, the application of an isolated lepton finder in the selection processor will largely veto the lνqqqq and llqqqq final states, therefore, the absence of weight information for these final states will not significantly affect the sensitivity measurement based on the $\nu\nu$qqqq final state.

Final State	Cross Section [fb] $(\alpha_4 = \alpha_5 = 0.00)$	Cross Section [fb] $(\alpha_4 = \alpha_5 = 0.05)$	Percentage Change[%]	CLIC Cross Section [fb]
$e^+e^- \to \nu\nu$qqqq	20.8	34.6	+66.3	24.7
$e^+e^- \to$ lνqqqq	112	113	+0.9	115.3
$e^+e^- \to$ llqqqq	59.7	68.6	+14.9	62.1

Table 1.1.: Cross section for selected processes for given value of α_4 and α_5 at 1.4 TeV.

Final State	Cross Section [fb] $(\alpha_4 = \alpha_5 = 0.000)$	Cross Section [fb] $(\alpha_4 = \alpha_5 = 0.005)$	Percentage Change[%]	CLIC Cross Section [fb]
$e^+e^- \to \nu\nu$qqqq	51.2	77.7	+51.8	71.5
$e^+e^- \to$ lνqqqq	111.9	115.9	+3.6	106.6
$e^+e^- \to$ llqqqq	169.7	161.7	-4.9	169.3

Table 1.2.: Cross section for selected processes for given value of α_4 and α_5 at 3 TeV.

1.3. Simulation and Reconstruction

The CLID_ILD detector [1] was simulated using MOKKA [10], a GEANT4 [2] wrapper providing detailed geometric descriptions of detector concepts for the linear collider. Events were reconstructed using MARLIN [5] a c++ framework designed for reconstruction at the linear collider. PandoraPFA [9, 14] is used to apply particle flow calorimetry to these samples and to produce PFOs that are used in this analysis.

Using the CLIC_ILD detector for this analysis provides access to the background samples created by the CLIC collaboration. The CLIC_ILD detector has a 60 layer scintillator-tugsten HCal in comparison to the 48 layer HCal found in the default

ILD detector. The increase in thickness of the detector for the CLIC experiment is needed to compensate for the effects of leakage at the higher energies seen by the CLIC experiment in comparison to the ILC. Practically speaking the ILD and CLIC_ILD detectors are otherwise identical.

1.3.1. Experimental Conditions at CLIC

The CLIC experiment will operate in a unique environment in comparison to previous generations of lepton colliders and these must be properly accounted for in any analysis to get a measure of the true physics potential CLIC has to offer. The following aspects of the CLIC experiment present the largest challenges to the physics potential for the CLIC experiment:

- The high bunch charge density. The small beam size at the impact point produces very large electromagnetic fields that interact with the particles from the opposite beam causing them to radiate photons. This effect is known as beamstrahlung and it acts to reduce the collision energy of the e^+e^- pairs.

- Beam related backgrounds. Beamstrahlung photons can further interact through a number of different mechanisms each of which contribute to different background processes that must be accounted for. Dominant processes that cannot be easily vetoed include incoherent pair production of e^+e^- and $\gamma\gamma \to$ Hadron.

- Fast readout technology is crucial. The CLIC bunch train consists of 312 bunches with a repetition rate of 50 Hz. Each bunch is separated by 0.5ns. As this is such a small separation it will be necessary to integrate over multiple bunch crossing when reading out the detectors. This places tight constraints on all detector electrical readout speeds and time resolutions.

1.3.2. Beam-Related Backgrounds at CLIC

The primary sources of background for the CLIC experiment are as follows:

- e^+e^- pair creation from the interaction of a beamstrahlung photons with the electromagnetic field from the opposite beam. The different mechanisms for pair creation are coherent, incoherent and trident pairs are pair production. Coherent pair production occurs when a real beamstrahlung photon interacts with the

electromagnetic field from the opposite beam, trident pair production occurs when a virtual beamstrahlung photon interacts with the electromagnetic field from the opposite beam and incoherent pair production occur when a real or virtual beamstrahlung photon interacts with the individual particles in the opposite beam.

- $\gamma\gamma \rightarrow$ Hadron from the interaction of real or virtual beamstrahlung photons with each other. Example Feynman diagrams for such processes is shown in figure ??.

- Beam halo muons that arise from inelastic collisions of the beam particles during collimation.

Each of these has to be properly addressed to get a true measure of the physics potential at CLIC. Coherent and trident pair production is not a dominant source of background as they are produced at low transverse momenta, as figure 1.2 shows, and a simple cut could veto these backgrounds. This is not the case for incoherent pair production of e^+e^-, which are dominant in the forward regions of the detector, and $\gamma\gamma \rightarrow$ Hadron, which are dominant in the tracker and the calorimeters (with the exception of low radii in the calorimeter endcaps) [8,12]. Beam halo muons prove not to be a dominant source of background either as, thanks to the unique topology of a muon passing through a detector it is possible to isolate them at PFO construction and remove them from further processing. A preliminary version of a processor designed for this purpose was implemented within PandoraPFA [8].

As $\gamma\gamma \rightarrow$ Hadron events deposit more energy than incoherent pair production [8], they are the most dominant background to consider. They are included into this analysis by overlaying $\gamma\gamma \rightarrow$ Hadron events onto the signal events. For each event the exact number of events overlaid is drawn from a Poisson distribution with a mean of 3.2(1.3) events per bunch crossing at 3(1.4) TeV. While incoherent pairs are still a source of background they will produce a second order effect in comparison to the $\gamma\gamma \rightarrow$ Hadron events.

The PFO choices described in section 1.7 are applied to veto PFOs that arise from the overlaid $\gamma\gamma \rightarrow$ Hadron events.

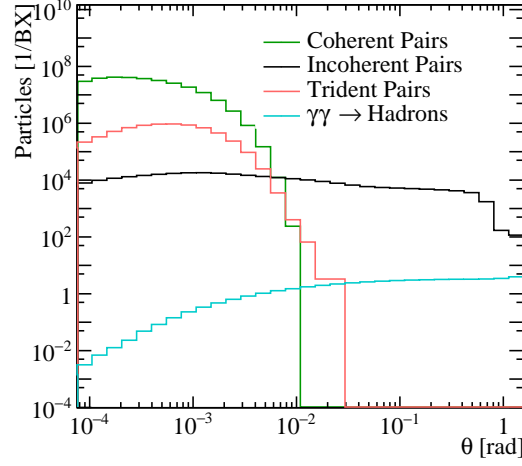**Figure 1.2.:** Angular distribution of number of particles for beam induced backgrounds for CLIC at $\sqrt{s} = 3$ TeV. Taken from CLIC CDR.

(a) Visible Mass

(b) $\cos\theta_{Missing}$ - The cosine of the polar angle of the missing momentum for an event.
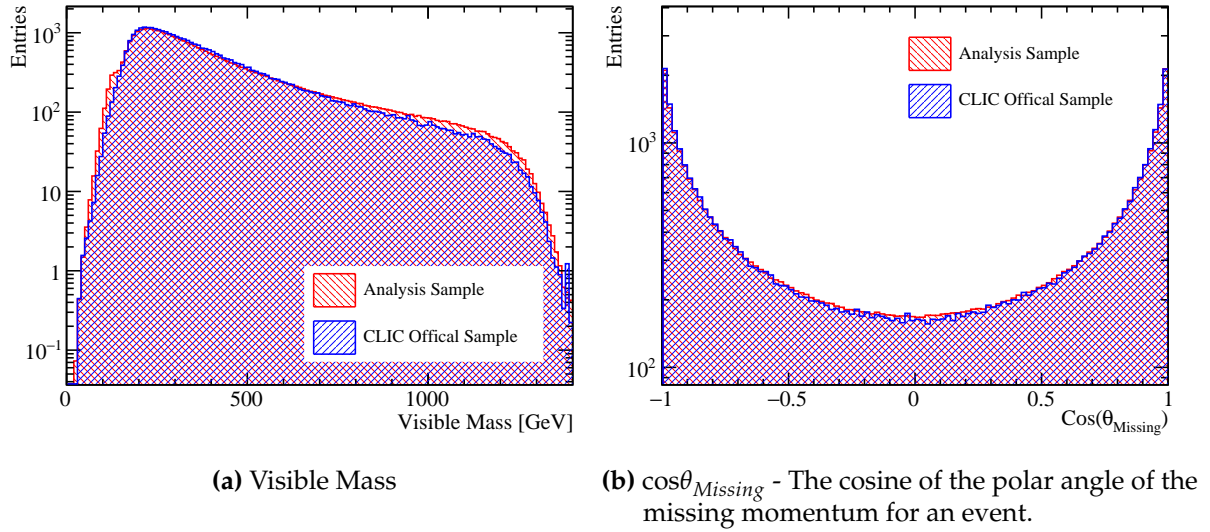
Figure 1.3.: Comparison of various distributions between samples used in this analysis and the official CLIC samples for the $\nu\nu qqqq$ final state.

1.4. Validation of New Samples

An identical setup to that used for the official CLIC sample was used for the event generation and reconstruction. Several reconstructed level distributions were compared to the official CLIC samples and all were found to be comparably to each other. A selection of these distributions is shown in figure 1.3.

1.5. Analysis Processor and Jet Pairing

For both signal and background events the MarlinFastJet processor, a wrapper for the FastJet [4] process, is used to cluster the events into 4 jets. These are jets assumed to be from the hadronic decays of the bosons involved in the vector scattering process. These jets are paired up such that on the assumption that the correct pair arises when the invariant masses of the two pairs are closest together. The longitudinally invariant kt jet algorithm in exclusive modes is used for the jet clustering. This jet algorithm proceeds as follows:

- For each pair of particles i and j work out the kt distance and beam distance $d_{iB} = p_t^2$.

$$d_{ij} = \min(p_{ti}^2, p_{tj}^2)\Delta R_{ij}^2 / R^2 \tag{1.1}$$

  where $\Delta R_{ij}^2 = (y_i - y_j)^2 + (\phi_i - \phi_j)^2$. p_t is the transverse momentum of the particle with respect to the beam axis, y_i is the rapidity of particle i and ϕ_i is the azimuthal angle of particle i. R is a configurable parameter that typically is of the order of 1.

- Find the minimum distance $d$min of all the k_t and beam distances. If the minima occurs for a k_t distance, merge particles i and j, summing their 4-momenta in the energy combination scheme (also configurable). If the beam distance is the minimum declare particle i to be apart of the "beam" jet and remove it from the list of particles and not included in the final output jets.

- Repeat until no particles are left or the requested number of jets have been created (or optionally apply a minimum d_{cut} where clustering stops, but here the event is forced into 4 jets).

An inclusive mode is available, but not applied here as the finally number of jets in the output varies and events need to be clustered into 4 jets for this analysis. Two other clustering modes were considered, but were found to be inappropriate for this analysis as is shown in figure 1.4. They were:

- The kt algorithm for e+e colliders (or Durham algorithm) where $d_{ij} = 2\min(E_i^2, E_j^2)(1 - cos\theta_{ij})$ and d_{iB} is not used. θ_{ij} is the opening angle of the particles. In the collinear limit this corresponds to the relative transverse momentum of the particles. Unlike the other algorithm choices this is not invariant to boosts along the beam
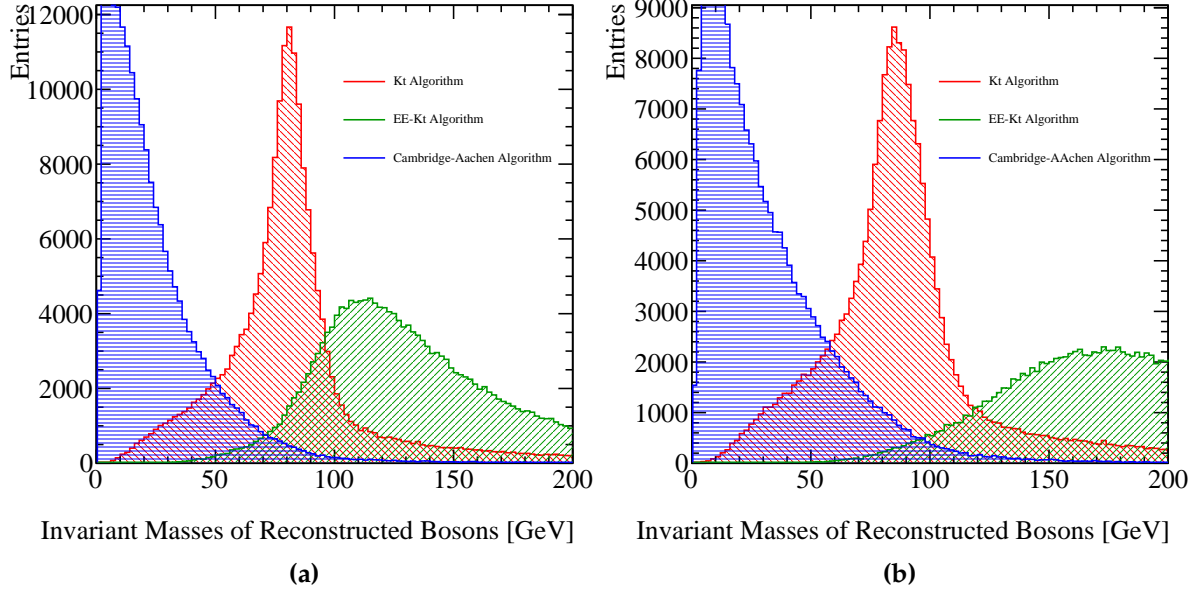
Figure 1.4.: Reconstructed masses for different choices of jet algorithm for 1.4 TeV and 3 TeV $\nu\nu qqqq$ events. These masses arise by forcing the reconstructed events into 4 jets and then pairing up the jets into pairs such that the reconstructed invariant masses of the pairs are closest to each other. These samples should be dominated by vector boson scattering involving pairs of W bosons and so it is expected that a peak at the W boson true mass should be observed. As this does not occur for the Cambridge-Aachen algorithm or the ee_kt algorithm they were deemed unsuitable for this analysis at both 1.4 and 3 TeV. In the case of the kt algorithm and the ee_kt algorithm an R parameter of 0.7 was used.

direction as in theory for e+e colliders the collision should occur with no net 3 momentum, unlike hadron colliders where the events have a net 3-momentum. However, the presence of ISR and beam effects makes this algorithm inappropriate for CLIC. The major failure of this algorithm choice is the absence of diB as this associates too many background particles to jets when applied at CLIC.

- The Cambridge/Aachen jet algorithm where $d_{ij} = \Delta R_{ij}^2 / R^2$ and $d_{iB} = 1$. This algorithm gave poor performance as it is based entirely on spacial information and does not account for the transverse momentum or energy of the particles being grouped. In essence this is a cone clustering algorithm with a cone radius defined through $\Delta R_{ij} = R$, which even for large R was found to throw away too much energy in the event to be useful for this analysis. This algorithm can be useful for events with small jets that are highly boosted, but in this case the jets are too large to be successfully merged.

An isolated lepton finder is included in the analysis chain in an attempt to reject background events containing leptons. The LCFIPlus [13] processor is also run on these events once clustered into jets to produce a value for the B and C tag likelihood for a jet.

This information is available for background rejection rather than contributing to the sensitivity of the event to the anomalous couplings. The LCFIPlus vertex processor was trained using events of $e^+e^- \rightarrow Z\nu\nu \rightarrow q\bar{q}\nu\nu$ for q = u,d,s,c,b.

Finally, an analysis processor is run, which calculates a number of variables used downstream in the analysis. Included in these are:

- Number of PFOs in the jets and the paired up bosons.

- Number of charged PFOs in the jets and paired up bosons.

- Highest energy PFO: energy, momentum, transverse momentum, $cos\theta$.

- Highest energy electron PFO: energy, momentum, transverse momentum, $cos\theta$.

- Highest energy muon PFO: energy, momentum, transverse momentum, $cos\theta$.

- Highest energy photon PFO: energy, momentum, transverse momentum, $cos\theta$.

- (If in existence) Highest and second highest energy isolated lepton: energy, momentum, transverse momentum, $cos\theta$.

- Bosons: energy, momentum, transverse momentum, $cos\theta$.

- Invariant mass of the boson pair.

- Jets: energy, momentum, transverse momentum, $cos\theta$.

- $Cos\theta$ Of the missing 3-momentum vector.

- Recoil mass.

- Invariant mass of the visible system.

- y_i, y_{i+1}. Jet clustering parameters ranging from i = 0 to 6.

- $Cos\theta^*_{Jet}$. This is the opening angle of a pair of jets, assumed to be from a signle boson, in the rest frame of the boson.

- $Cos\theta^*_{Boson}$. This is the opening angle of a pair of bosons, assumed to be from vector boson scattering, in the rest frame of the di-boson pair.

- Transverse momentum and energy of the event.

- Acolinearity of the jet pairs forming the bosons and the acoilinearity of the boson pair.

- Principle thrust T and the thrust axes $\bar{\mathbf{n}}$. Note $\bar{\mathbf{n}}$ is a unit vector. These are defined by the following equation

$$T = \max_{\bar{\mathbf{n}}}\left(\frac{\Sigma_i \mathbf{p}_i.\bar{\mathbf{n}}}{\Sigma_i |\mathbf{p}_i|^2}\right) \tag{1.2}$$

- The major and minor thrust values. These are defined with respect to the thrust axes $\bar{\mathbf{n}}$ in the following way:

$$T = \max_{\bar{\mathbf{n}}_{major}}\left(\frac{\Sigma_i \mathbf{p}_i.\bar{\mathbf{n}}_{major}}{\Sigma_i |\mathbf{p}_i|^2}\right) \tag{1.3}$$

where $\bar{\mathbf{n}}_{major}.\bar{\mathbf{n}} = \mathbf{0}$. Similarly the minor thrust value is defined as

$$T = \frac{\Sigma_i \mathbf{p}_i.\bar{\mathbf{n}}_{minor}}{\Sigma_i |\mathbf{p}_i|^2} \tag{1.4}$$

where $\bar{\mathbf{n}}_{minor}.\bar{\mathbf{n}} = \bar{\mathbf{n}}_{minor}.\bar{\mathbf{n}}_{major} = \mathbf{0}$

- Sphericity. This is defined using the sphericity tensor S^{ab} defined as:

$$S^{ab} = \frac{\Sigma_i p_i^\alpha p_j^\alpha}{\Sigma_{i,\alpha=1,2,3} |p_i^\alpha|^2} \tag{1.5}$$

Where p_i are the components of the momenta of particle i in the frame of the detector and the sum runs over all particles in the event. Sphericity is defined as $S = \frac{3}{2}(\lambda_2 + \lambda_3)$, where λ_i are the eigenvalues of the sphericity tensor defined such $\lambda_1 \geq \lambda_2 \geq \lambda_3$. This provides a measure of how spherical the reconstructed event topology is with isotropic events having $S \approx 1$, while two jet events have $S \approx 0$. (Also $\lambda_1 + \lambda_2 + \lambda_3 = 1$.)

- Aplanarity. Aplanarity is defined as $\frac{3}{2}\lambda_3$ where λ_3 is an eigenvalue of the sphericity tensor. This provides a measure of whether an event is linear or planar.

- B and C tag values for the jets, the min and max B and C tag values for the bosons.

Alongside these variables, for the $\nu\nu qqqq$ final state a number of Monte-Carlo variables are calculated for informative purposes and are not used in the analysis. These include:

- The quark and neutrino 4 momenta.

- Invariant mass of boson pair using MC pairing and MC energy.

- Invariant mass of boson pair using MC pairing and reconstructed jet energy.

1.6. Methodology for Fitting

It is necessary to discuss the fitting procedure in this analysis as the optimisation of the jet algorithms relies on this methodology. In this section only the signal events are considered to determine the underlying sensitivity of the CLIC detector to the anomalous couplings. This decision was made to save analysis of the large number of background samples in the optimisation of the jet reconstruction algorithms, while still optimising the algorithm on the physics of interest.

1.6.1. Choice of Fitting Distribution

The sensitivity of CLIC to the anomalous gauge couplings is determined through the use of a χ^2 fit to the distribution of $\cos\theta^*_{Jets}$ where θ^*_{Jets} is the angle between the two jets produced from the hadronic decay of the W/Z boson in the rest frame of that boson. The distribution of $\cos\theta^*_{Jets}$ proved to be sensitive to the anomalous gauge couplings as shown in figure 1.5.

Another distribution considered for the sensitivity study was $\cos\theta^*_{Bosons}$ where θ^*_{Bosons} is the angle between the two bosons produced in vector boson scattering in the rest frame of the boson pair. This distribution was found to be less sensitive to the anomalous gauge couplings than $\cos\theta^*_{Jets}$, which can be seen when comparing figures 1.5 and 1.6, and so was not considered for the rest of this study. Furthermore, it was found that a two dimensional χ^2 fit produced by combining $\cos\theta^*_{Jets}$ and $\cos\theta^*_{Bosons}$ did not improve the sensitivity significantly in comparison to $\cos\theta^*_{Jets}$.

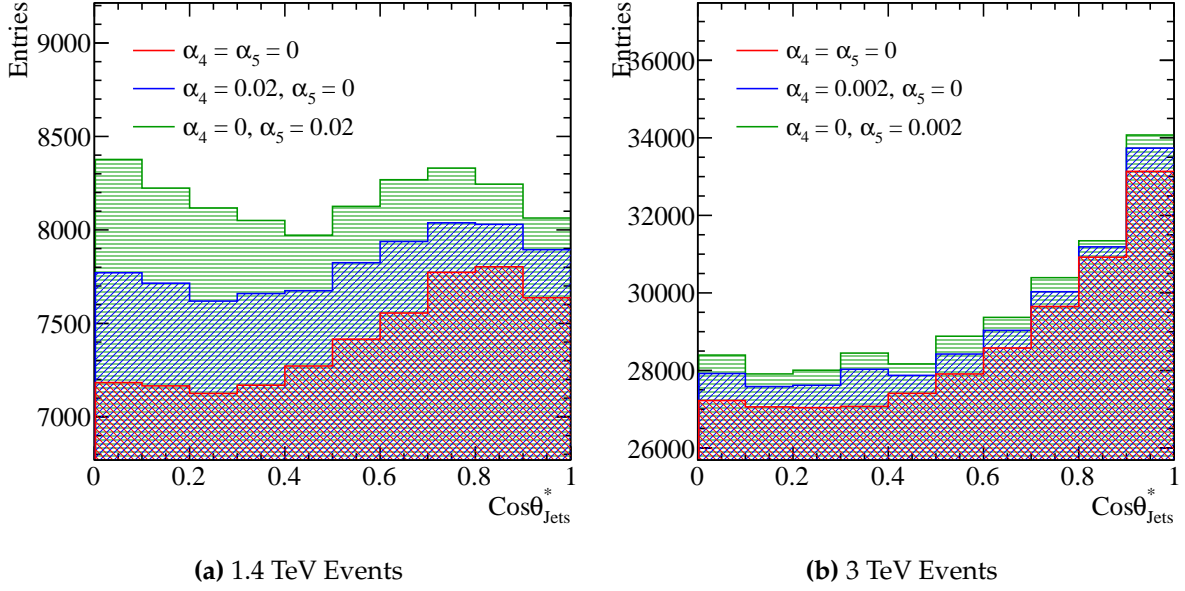**(a)** 1.4 TeV Events   **(b)** 3 TeV Events

Figure 1.5.: Sensitivity of $\cos\theta^*_{Jets}$ to anomalous couplings at 1.4 and 3 TeV. The jet algorithm used for this example was the longitudinally invariant kt algorithm with an R parameter of 0.7. This sample corresponds to pure signal of hadronic decays in vector boson scattering i.e. $\nu\nu qqqq$.

The $\cos\theta^*_{Jets}$ variable was binned in histograms of 10 bins before begin converted into a value of χ^2. This binning was selected to maximise the number of bins in the distribution, while minimising the effect of large bin by bin fluctuations arising from individual events with large event weights.

1.6.2. Event Weight Impact on Fitting Distribution

At 1.4 TeV event weights were produced from Whizard stepping along α_4 and α_5 in steps of 0.01 ranging from -0.07 to 0.07 as shown in figure 1.4, however, to produce a smooth χ^2 contour much finer sampling is needed. While it is feasible to generate new event weights in Whizard for any pair of α_4 and α_5 it is time consuming making it impractical for this analysis. To overcome this difficulty bicubic interpolation is applied between these points to allow for the extract of event weights anywhere within the range -0.05 to 0.05. As figure 1.7 shows the interpolated surface proves to be a good fit to the data produced from the generator in that it is smooth and continuous.
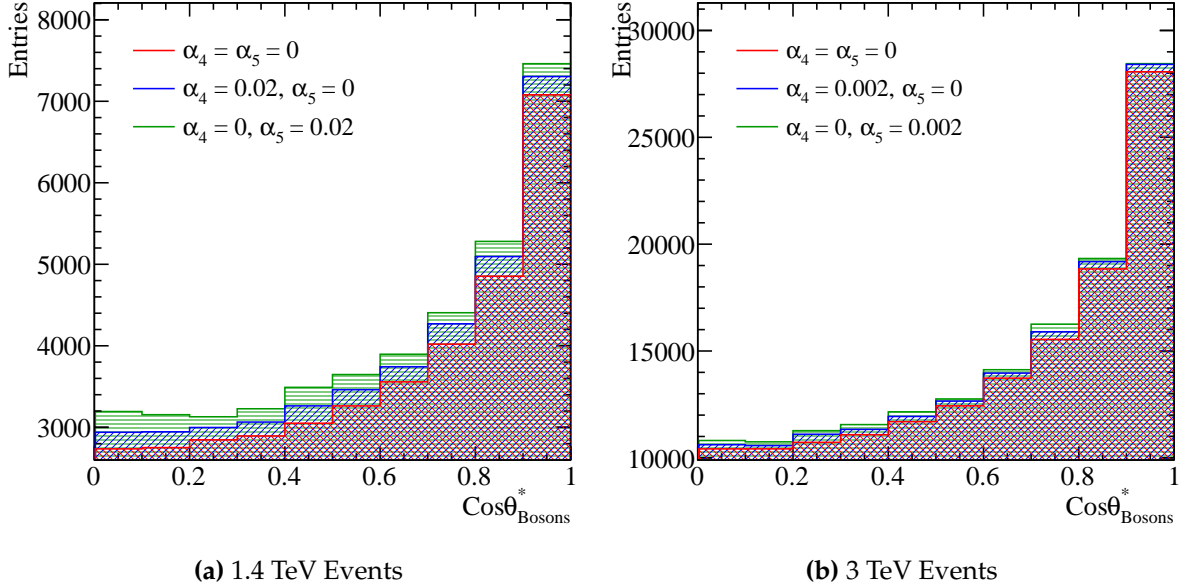
(a) 1.4 TeV Events   **(b)** 3 TeV Events

Figure 1.6.: Sensitivity of $\cos\theta^*_{Bosons}$ to anomalous couplings at 1.4 and 3 TeV. The jet algorithm used for this example was the longitudinally invariant kt algorithm with an R parameter of 0.7. This sample corresponds to pure signal of hadronic decays in vector boson scattering i.e. $\nu\nu qqqq$.

Similarly at 3 TeV the same procedure was used but stepping occurs in steps of 0.001 ranging from -0.007 to 0.007 in both α_4 and α_5. These ranges proved to be sufficient for the contours of interest for the CLIC sensitivity analysis at this energy.

1.6.3. Analysis of Fitting Distribution

Using these interpolated surfaces for the event weights, distribution of $\cos\theta^*_{Jets}$ were produced stepping across α_4 and α_5 in steps of 0.0001 at 1.4 TeV and 0.00001 at 3 TeV. Each distribution was converted into a value of χ^2 using the following formula:

$$\chi^2 = \Sigma_i \frac{(O_i - E_i)^2}{E_i} \tag{1.6}$$

where O_i is the observed bin content for bin i in the distribution with non-zero α_4 and α_5 and E_i is the expected bin content for bin i in the distribution with zero α_4 and α_5 i.e. the standard model expected value.

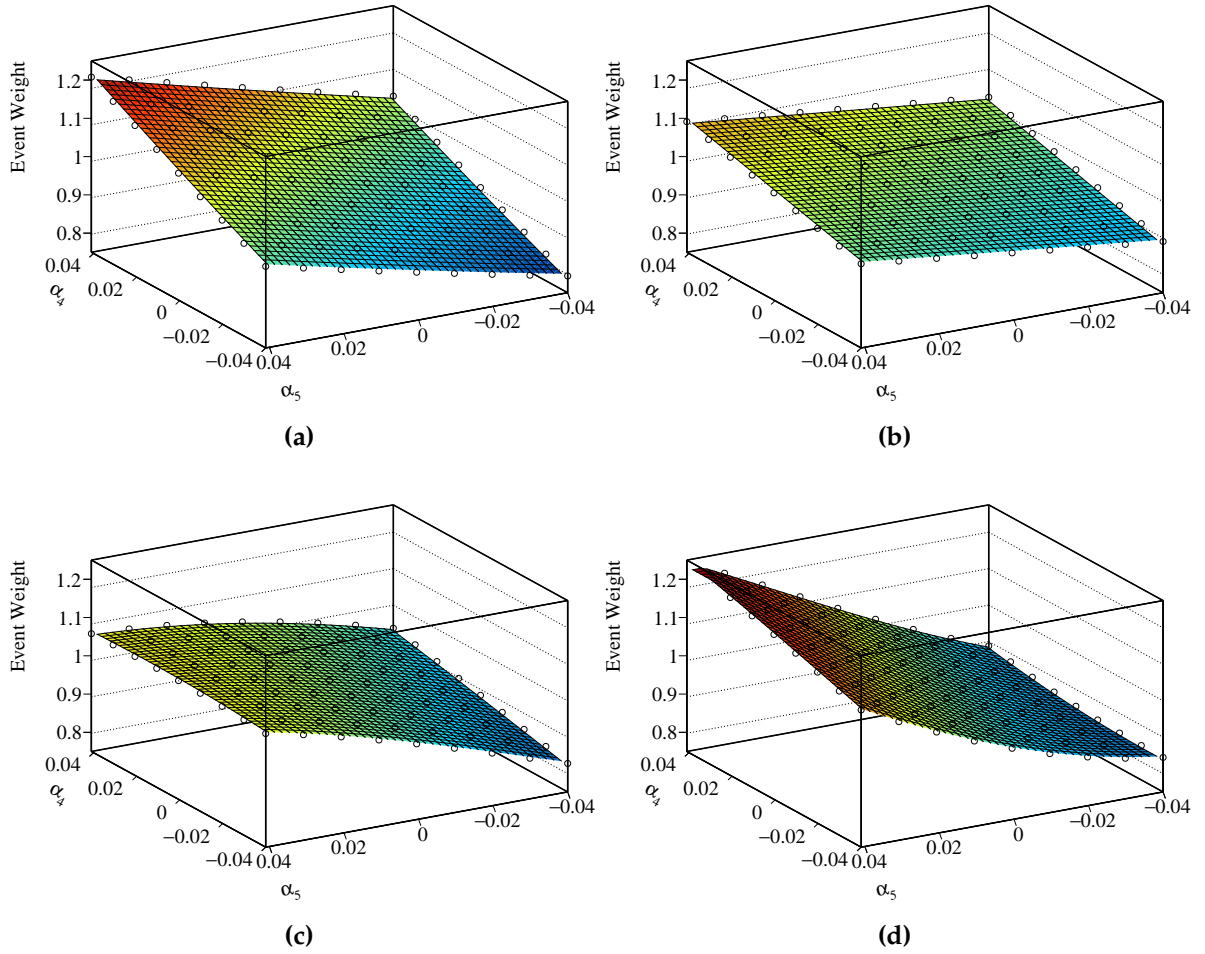**(a)**

(b)

(c)

(d)

Figure 1.7.: A selection of plots showing how the event weight changes when varying the anomalous couplings α_4 and α_5 for 1.4TeV $\nu\nu$qqqq final state events. The hollow circles show the event weight produced from the generator while the surface shown is found using bicubic interpolation between those points.

Confidence limits indicate the probability of measuring a given value of χ^2 in the α_4 and α_5 space. The confidence limits used in subsequent sections, 68%, 90% and 99% are defined using constant χ^2 contours of 2.28, 4.61 and 9.21, which arise from the integral of the two dimensional χ^2 function.

It is useful to reduce these distributions to sensitivities to the individual parameters α_4 and α_5 independently. This is done by projecting out either the $\alpha_4 = 0$ or $\alpha_5 = 0$ one dimensional χ^2 distribution from the two dimensional χ^2 distribution. Using these one dimensional plots it is possible to extract the sensitivity to an individual parameters using confidence limits arising from the integral of the two dimensional χ^2 function i.e. 68% confidence limit occurs for $\chi^2 = 0.989$. In subsequent chapters these are the sensitivities quoted for individual anomalous gauge coupling parameters.

1.7. Optimisation of Jet Reconstruction

The jet algorithm used for this analysis is the longitudinally invariant kt algorithm as described in section 1.5. The parameter choices under consideration for optimisation are the R parameter, used in the kt algorithm definition, used and the PFO selection.

A number of cuts [9] are applied to the transverse momenta and the time of the PFOs produced by PandoraPFA to reduce the PFOs into a subset that are believed to originate from the desired interaction in an attempt to veto the overlaid $\gamma\gamma \to$ Hadron background events. Different options for these cuts give rise to the tight, default and loose selected PFOs that are considered in this optimisation.

The optimal sensitivity is achieved for either loose selected PFOs with an R parameter of 0.7 or default selected PFOs with an R parameter of 0.9 as can be seen from tables 1.3 and 1.4. As a tie breaker between these options the separation power, the fraction of events misidentified as either arising from a WW pair or a ZZ pair, was considered. Again performance was similar, but there was a slight preference towards the use of selected PFOs and an R parameter of 0.9. While not used in the primary analysis the separation of samples into WW and ZZ events is important for an extension analysis found in section BLAH.

The optimal contours can be found in figure 1.8 and the optimal 1D plot used to produce the errors references in the tables 1.3 and 1.4 can be found in figures 1.9 and

1.10 respectively. All other contours and plots for this optimisation can be found in the appendices.

PFO Selection R Parameter	Tight Selected PFOs	Selected PFOs	Loose Selected PFOs
0.7	$-0.0039 +0.0050$	$-0.0038 +0.0050$	$-0.0037 +0.0046$
0.9	$-0.0041 +0.0051$	$-0.0038 +0.0046$	$-0.0038 +0.0048$
1.1	$-0.0041 +0.0051$	$-0.0039 +0.0050$	$-0.0040 +0.0050$

Table 1.3.: Precision on measurement of α_4 at 1.4 TeV for different jet reconstruction parameters considering pure signal and applying a χ^2 fit to $\cos\theta^*_{Jets}$.

PFO Selection R Parameter	Tight Selected PFOs	Selected PFOs	Loose Selected PFOs
0.7	$-0.0027 +0.0031$	$-0.0027 +0.0032$	$-0.0025 +0.0030$
0.9	$-0.0028 +0.0032$	$-0.0026 +0.0030$	$-0.0026 +0.0030$
1.1	$-0.0028 +0.0032$	$-0.0027 +0.0032$	$-0.0028 +0.0031$

Table 1.4.: Precision on measurement of α_5 at 1.4 TeV for different jet reconstruction parameters considering pure signal and applying a χ^2 fit to $\cos\theta^*_{Jets}$.

PFO Selection R Parameter	Tight Selected PFOs	Selected PFOs	Loose Selected PFOs
0.7	$-0.00051 +0.000508$	$-0.000477 +0.000487$	$-0.000531 +0.000539$
0.9	$-0.000548 +0.000541$	$-0.000519 +0.000505$	$-0.000550 +0.000539$
1.1	$-0.000446 +0.00045$	$-0.000481 +0.000466$	$-0.000478 +0.000467$

Table 1.5.: Precision on measurement of α_4 at 3 TeV for different jet reconstruction parameters considering pure signal and applying a χ^2 fit to $\cos\theta^*_{Jets}$.

1.8. Event Selection

As discussed earlier the signal events for this analysis contain the $\nu\nu qqqq$ final state. The processes to be considered in this analysis alongside the signal are events that
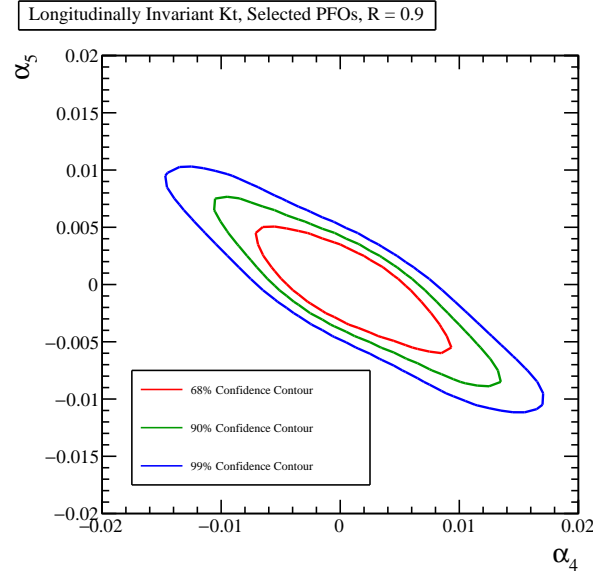
Figure 1.8.: χ^2 Sensitivity contours for the $qqqq\nu\nu$ final state arising from a fit to $\cos\theta^*_{\text{Jets}}$ at 1.4 TeV for the optimal jet reconstruction parameters.
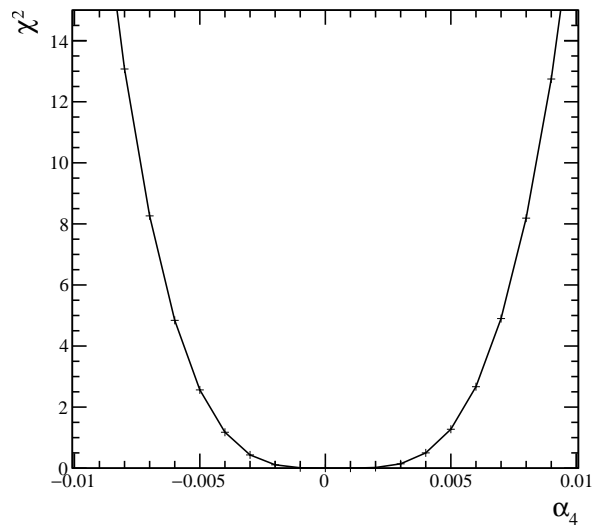

Figure 1.9.: χ^2 as a function of α_4 assuming $\alpha_5 = 0$ for the $qqqq\nu\nu$ final state arising from a fit to $\cos\theta^*_{\text{Jets}}$ at 1.4 TeV for the optimal jet reconstruction parameters.
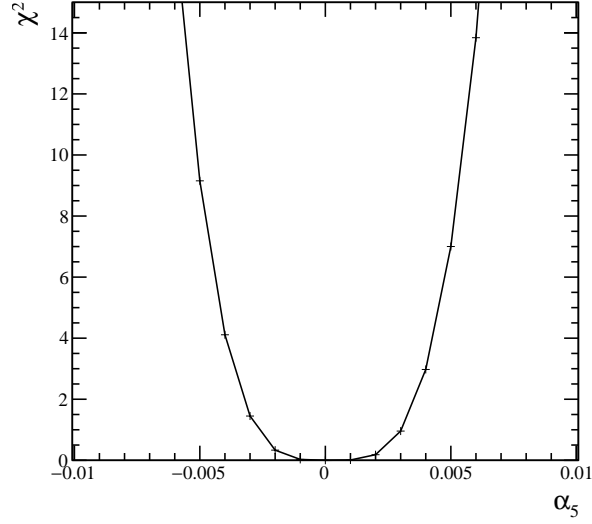
Figure 1.10.: χ^2 as a function of α_5 assuming $\alpha_4 = 0$ for the qqqq$\nu\nu$ final state arising from a fit to $\cos\theta^*_{\text{Jets}}$ at 1.4 TeV for the optimal jet reconstruction parameters.

PFO Selection	Tight Selected PFOs	Selected PFOs	Loose Selected PFOs
R Parameter			
0.7	$-0.000375\ +0.000358$	$-0.000350\ +0.000343$	$-0.000346\ +0.00034$
0.9	$-0.000378\ +0.000355$	$-0.000376\ +0.000351$	$-0.000379\ +0.000358$
1.1	$-0.000339\ +0.000328$	$-0.000358\ +0.000343$	$-0.000339\ +0.000326$

Table 1.6.: Precision on measurement of α_5 at 3 TeV for different jet reconstruction parameters considering pure signal and applying a χ^2 fit to $\cos\theta^*_{Jets}$.

would topologically look similar to signal in the detector. This includes events that could be confused with 4 jet events with missing energy, while excluding those events with large numbers of high energy leptons that could be vetoed easily during the analysis stage. In full the list includes:

EPA (equivalent photon approximation) processes model the electromagnetic field of a charged particle as virtual photons. BS (beamstrahlung) processes involve photons that have been radiated from incoming charged particles due to interactions with the electromagnetic field of the opposite beam. The energy spectrum of the incoming particles for CLIC at the relevant operating energy is used to model the energy of these incoming photons. Included in this study are photon-photon interactions from photons appearing from the EPA and beamstrahlung processes.

Final State	Cross Section 1.4 TeV [fb]	Cross Section 3 TeV [fb]
$e^+e^- \to \nu\nu qqqq$	24.7	71.5
$e^+e^- \to l\nu qqqq$	110.4	106.6
$e^+e^- \to llqqqq$	62.1	169.3
$e^+e^- \to qqqq$	1245.1	546.5
$e^+e^- \to \nu\nu qq$	787.7	546.5
$e^+e^- \to l\nu qq$	4309.7	5560.9
$e^+e^- \to llqq$	2725.8	3319.6
$e^+e^- \to qq$	4009.5	2948.9
$\gamma_{EPA}e^- \to qqqqe^-$	287.1	287.8
$\gamma_{BS}e^- \to qqqqe^-$	1160.7	1268.6
$e^+\gamma_{EPA} \to qqqqe^+$	286.9	287.8
$e^+\gamma_{BS} \to qqqqe^+$	1156.3	1267.3
$\gamma_{EPA}e^- \to qqqq\nu$	32.6	54.2
$\gamma_{BS}e^- \to qqqq\nu$	136.9	262.5
$e^+\gamma_{EPA} \to qqqq\nu$	32.6	54.2
$e^+\gamma_{BS} \to qqqq\nu$	136.4	262.3
$\gamma_{EPA}\gamma_{EPA} \to qqqq$	753.0	402.7
$\gamma_{EPA}\gamma_{BS} \to qqqq$	4034.8	2423.1
$\gamma_{BS}\gamma_{EPA} \to qqqq$	4018.7	2420.6
$\gamma_{BS}\gamma_{BS} \to qqqq$	21406.2	13050.3

Table 1.7.: Cross sections of signal and background processes at 1.4 and 3 TeV. In the above table $q \in u, \bar{u}, d, \bar{d}, s, \bar{s}, c, \bar{c}, b$ or $\bar{b}$ while $l \in e^\pm, \mu^\pm$ or $\tau^\pm$ and $\nu \in \nu_e, \nu_\mu$ and ν_τ. The subscript EPA or BS for the incoming photons indicate whether the photon is generated from the equivalent photon approximation or beamstrahlung.

1.8.1. Pre Selection - 1.4 TeV

The primary selection of the $\nu\nu qqqq$ signal will be done using a multivariate analysis, however, in an attempt to veto trivial backgrounds a simple cut based preselection is applied. Cuts are applied to the transverse momentum, invariant mass of the visible system and the number of isolated leptons. The raw distributions of these variables is shown in figures 1.11, 1.12 and 1.13. Based on these distributions the following cuts were applied:
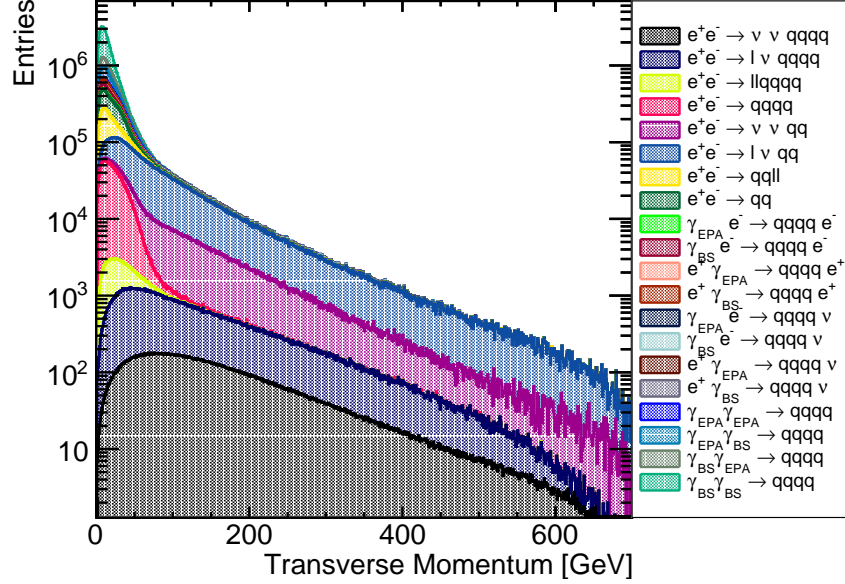
Figure 1.11.: The transverse momentum of signal and background events at 1.4 TeV.

- Transverse momentum > 100 GeV. This cut is effective due to the presence of missing energy in the form of neutrinos in the signal final state.

- Visible mass of the system > 200 GeV. This cut is effective for accounting for the missing energy of the neutrinos in the final state along the longitudinal direction of the detector instead.

- Number of isolated leptons = 0. This cut vetos a large number of events with leptons in the final state. The effect of these preselection cuts can be found in table 1.3. While a large fraction of the signal events are lost through these cuts, particularly the transverse momentum cuts, a much large fraction of background events are removed justifying the cut.

The event numbers for the signal and background are shown in table 1.8 as these cuts are cumulatively applied. These numbers are normalised to the correct luminosity for CLIC running at 1.4 TeV. As is expected the large transverse momentum cut removes practically all backgrounds containing no missing energy. The invariant mass cut removes significant fractions of two quark and missing energy events. Finally, the isolated lepton finder cut removes backgrounds containing visible leptonic final states.
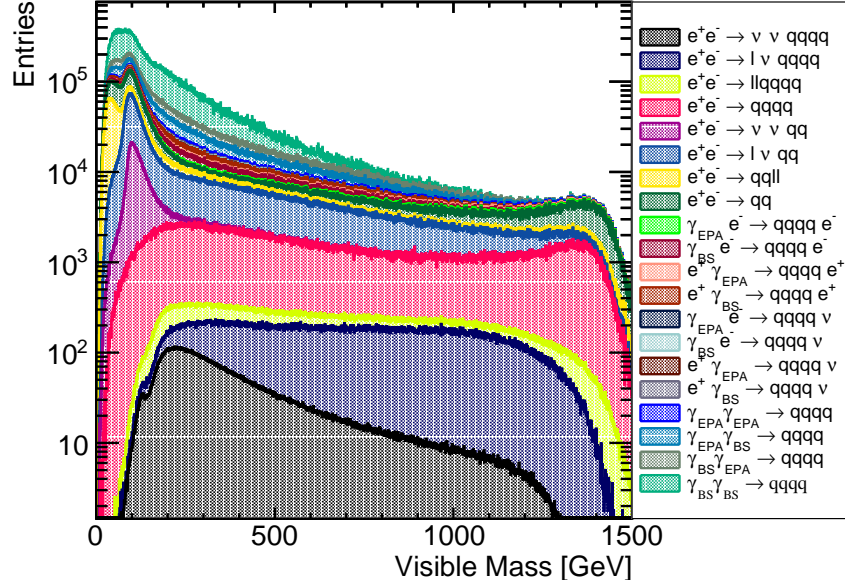
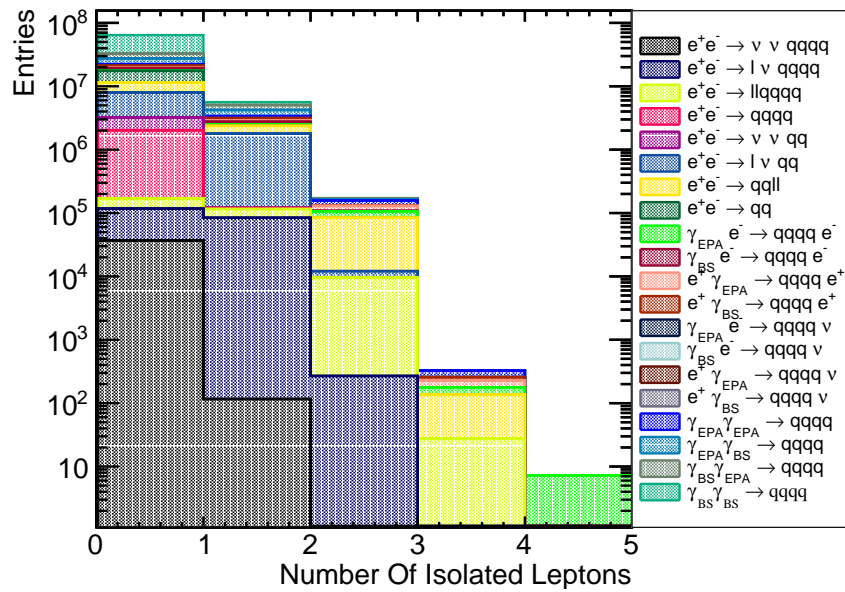**Figure 1.12.:** The invariant mass of the visible system of signal and background events at 1.4 TeV.

Figure 1.13.: The number of isolated leptons for signal and background events at 1.4 TeV.

Final State	Raw Event Numbers	$p_T > 100$ GeV	$p_T > 100$ GeV & $M_{\text{Vis}} > 200$ GeV	$p_T > 100$ GeV & $M_{\text{Vis}} > 200$ GeV & $N_{\text{Isolated Leptons}} = 0$
$e^+e^- \to \nu\nu qqqq$	37,050	23,782	21,091	21,034
$e^+e^- \to l\nu qqqq$	165,600	81,631	80,827	42,332
$e^+e^- \to llqqqq$	93,150	1,154	1,142	710
$e^+e^- \to qqqq$	1,867,631	6,755	6,742	6,729
$e^+e^- \to \nu\nu qq$	1,181,218	514,701	49,692	49,586
$e^+e^- \to l\nu qq$	6,463,852	2,002,405	1,258,172	568,450
$e^+e^- \to llqq$	4,088,143	7,656	7,263	5,651
$e^+e^- \to qq$	6,010,154	34,123	33,679	33,605
$\gamma_{\text{EPA}}e^- \to qqqqe^-$	430,643	2,301	2,294	762
$\gamma_{\text{BS}}e^- \to qqqqe^-$	1,741,050	1,773	1,688	1,294
$e^+\gamma_{\text{EPA}} \to qqqqe^+$	430,344	2,787	2,774	1,057
$e^+\gamma_{\text{BS}} \to qqqqe^+$	1,734,450	814	784	552
$\gamma_{\text{EPA}}e^- \to qqqq\nu$	48,893	17,468	13,558	8,895
$\gamma_{\text{BS}}e^- \to qqqq\nu$	205,326	75,429	48,648	48,023
$e^+\gamma_{\text{EPA}} \to qqqq\nu$	48,893	17,656	13,588	8,951
$e^+\gamma_{\text{BS}} \to qqqq\nu$	204,581	74,890	48,457	47,903
$\gamma_{\text{EPA}}\gamma_{\text{EPA}} \to qqqq$	1,129,459	3,126	3,018	1,421
$\gamma_{\text{EPA}}\gamma_{\text{BS}} \to qqqq$	6,052,200	7,205	7,059	5,531
$\gamma_{\text{BS}}\gamma_{\text{EPA}} \to qqqq$	6,027,979	5,187	5,116	3,197
$\gamma_{\text{BS}}\gamma_{\text{BS}} \to qqqq$	32,109,300	4,421	4,421	3,617

Table 1.8.: Number of events passing the various cuts applied in the preselection at 1.4TeV. Event numbers are normalised to the correct luminosity for CLIC at 1.4 TeV. p_T is the transverse momentum of the event, M_{Vis} is the visible mass and $N_{\text{Isolated Leptons}}$ is the number of isolated leptons in the event. In the above table $q \in$ u, ū, d, d̄, s, s̄, c, c̄, b or b̄ while $l \in$ e$^\pm$, $\mu^\pm$ or $\tau^\pm$ and $\nu \in \nu_e$, ν_μ and ν_τ. The subscript EPA or BS for the incoming photons indicate whether the photon is generated from the equivalent photon approximation or beamstrahlung.

1.8.2. MVA - 1.4 TeV

A multivariate analysis was applied to the data set to refine the selection using the TMVA toolkit [6]. The following variables were used for training the TMVA selection.

- Number of PFOs in the event.

- Highest energy PFO type.

- Transverse momentum of the event.

- $\cos\theta_{Missing}$. The cosine of the polar angle of the missing momentum.

- $\cos\theta_{\text{Highest Energy Track}}$. The cosine of the polar angle of the track with the largest momentum.

- y_i, y_{i+1}. Jet clustering parameters ranging from i = 0 to 6.

- Principle thrust, sphericity and aplanarity as defined in section BLAH.

- Energy of the highest energy electron in the event.

- Energy of the highest energy PFO in the event.

- Energy of the reconstructed bosons.

- Acolinearity of the reconstructed boson pair.

- Invariant mass of the reconstructed bosons.

- Acolinearity of the jets forming the reconstructed bosons.

It was found that the best MVA algorithm for both performance and speed was the booted decision tree (BDT) when comparing different methods using the default settings. Add plot here.

The BDT was further optimised by varying the number of trees used, the depth of the trees and the number of cuts applied. The results shown in the rest of this section use the optimal configuration. For the optimal BDT configuration a significance of $S/\sqrt{(S + B)} = 49.7$ was obtained.

The event numbers passing the BDT cut can be found in table 1.9. The performance of the BDT is shown in figure 1.14, which shows the change in the distribution of the the invariant mass of the reconstructed bosons as the MVA is applied. As expected the dominant background processes after the MVA is applied are those that will look identical to the visible signal process i.e. qqqq and missing energy. Two smaller sources of background that pass the MVA exists, those where two jets and missing energy are confused as four jets and missing energy and those where a lepton is not properly reconstructed and the events look like four jets and missing energy.
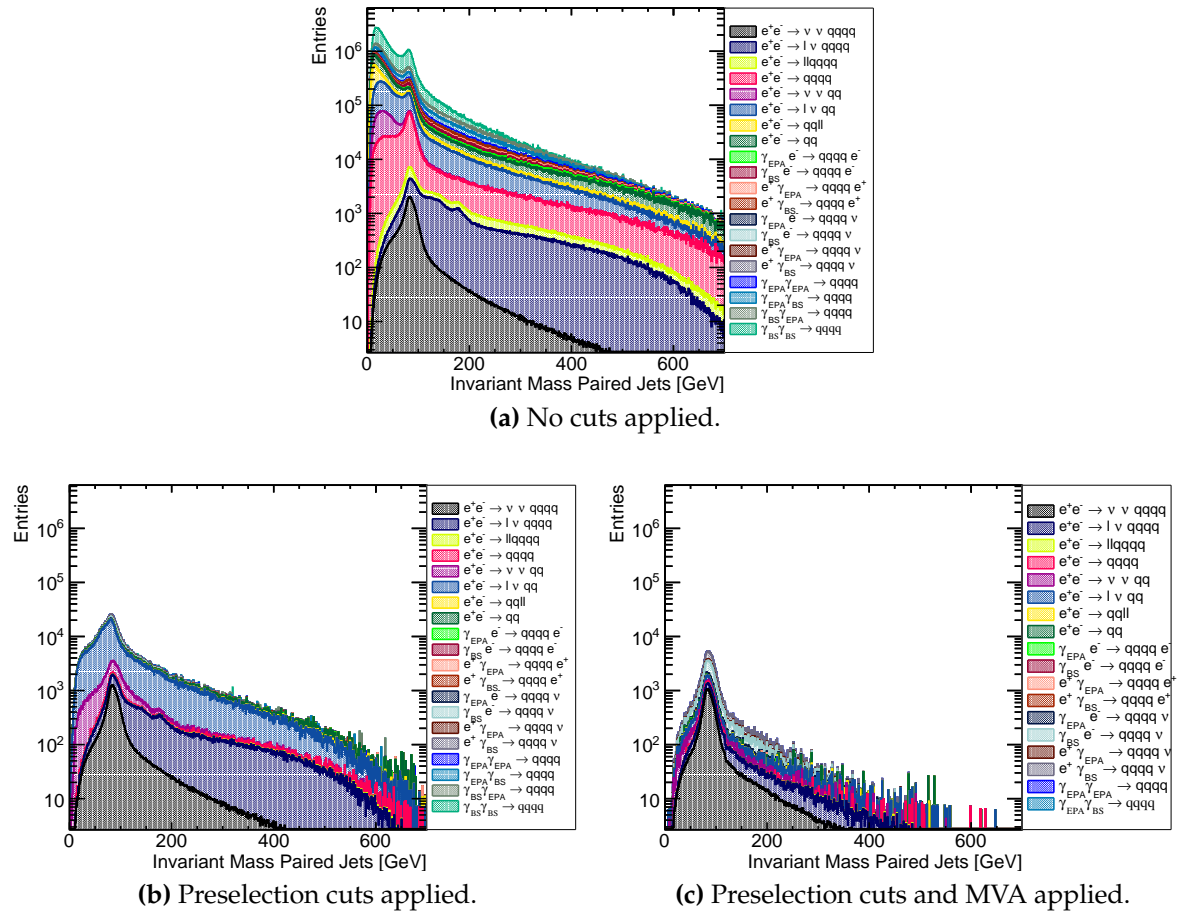
(a) No cuts applied.

(b) Preselection cuts applied.

(c) Preselection cuts and MVA applied.

Figure 1.14.: Impact of preselection and MVA on the reconstructed invariant mass of the bosons arising from jet pairing at 1.4 TeV.

Final State	Raw Event Numbers	Post MVA Selection Numbers
$e^+e^- \to \nu\nu qqqq$	37,050	15,167
$e^+e^- \to l\nu qqqq$	165,600	6,744
$e^+e^- \to llqqqq$	93,150	90
$e^+e^- \to qqqq$	1,867,631	1,417
$e^+e^- \to \nu\nu qq$	1,181,218	3,648
$e^+e^- \to l\nu qq$	6,463,852	7,169
$e^+e^- \to llqq$	4,088,143	296
$e^+e^- \to qq$	6,010,154	1,184
$\gamma_{EPA}e^- \to qqqqe^-$	430,643	27
$\gamma_{BS}e^- \to qqqqe^-$	1,741,050	113
$e^+\gamma_{EPA} \to qqqqe^+$	430,344	25
$e^+\gamma_{BS} \to qqqqe^+$	1,734,450	58
$\gamma_{EPA}e^- \to qqqq\nu$	48,893	3,728
$\gamma_{BS}e^- \to qqqq\nu$	205,326	25,723
$e^+\gamma_{EPA} \to qqqq\nu$	48,893	3,776
$e^+\gamma_{BS} \to qqqq\nu$	204,581	25,842
$\gamma_{EPA}\gamma_{EPA} \to qqqq$	1,129,459	81
$\gamma_{EPA}\gamma_{BS} \to qqqq$	6,052,200	73
$\gamma_{BS}\gamma_{EPA} \to qqqq$	6,027,979	0
$\gamma_{BS}\gamma_{BS} \to qqqq$	32,109,300	0

Table 1.9.: Number of events passing the MVA selection at 1.4TeV. Event numbers are normalised to the correct luminosity for CLIC at 1.4 TeV. The subscript EPA or BS for the incoming photons indicate whether the photon is generated from the equivalent photon approximation or beamstrahlung.

The summary of the selection procedure is given in table .

Final State	ϵ_{presel}	ϵ_{BDT}	N_{BDT}
$e^+e^- \to \nu\nu qqqq$	56.8%	40.9%	15,167
$e^+e^- \to l\nu qqqq$	25.6%	4.1%	6,744
$e^+e^- \to \nu\nu qq$	4.2%	0.3%	3,648
$e^+e^- \to l\nu qq$	8.8%	0.1%	7,169
$\gamma_{\text{EPA}}e^- \to qqqq\nu$	18.2%	7.6%	3,728
$\gamma_{\text{BS}}e^- \to qqqq\nu$	23.4%	12.5%	25,723
$e^+\gamma_{\text{EPA}} \to qqqq\nu$	18.3%	7.7%	3,776
$e^+\gamma_{\text{BS}} \to qqqq\nu$	23.4%	12.6%	25,842

Table 1.10.: Selection summary at 1.4TeV. The subscript EPA or BS for the incoming photons indicate whether the photon is generated from the equivalent photon approximation or beamstrahlung.

1.8.3. Pre Selection - 3 TeV

1.8.4. MVA - 3 TeV

1.9. Results

Appendix A.

Pointless extras

"Le savant n'étudie pas la nature parce que cela est utile;
   il l'étudie parce qu'il y prend plaisir,
   et il y prend plaisir parce qu'elle est belle."
   — Henri Poincaré, 1854–1912

Appendixes (or should that be "appendices"?) make you look really clever, 'cos it's like you had more clever stuff to say than could be fitted into the main bit of your thesis. Yeah. So everyone should have at least three of them...

A.1. Anomalous Gauge Coupling Quartic Vertices Of Relevance in Vector Boson Scattering

The anomalous gauge couplings involving α_4 and α_5 arise in EFT through the addition of the following terms to the Lagrangian.

$$\text{Tr}(V^\mu V_\nu)]\text{Tr}(V^\nu V_\mu)] \text{ and } [\text{Tr}(V^\mu V_\mu)]^2 \tag{A.1}$$

Where V_μ is defined in the following way.

$$V_\mu = \Sigma(D_\mu\Sigma)^\dagger \tag{A.2}$$

and Σ, the Higgs field matrix, is defined as.

$$\Sigma = \exp(-\frac{i}{v}\mathbf{w}) \tag{A.3}$$

Where $\mathbf{w} = w^a\sigma^a$. w^a are the ... and σ^a are the Pauli spin matrices. The covariant derivative of the Higgs field matrix is

$$D_\mu\Sigma = (\partial_\mu + \frac{ig}{2}W_\mu - \frac{ig'}{2}B_\mu\sigma^3)\Sigma \tag{A.4}$$

For clarity consider the unitarity gauge where $\mathbf{w} = 0$, which implies $\Sigma = 1$. In this gauge V_μ takes the following form.

$$V_\mu = \frac{i}{2}(gW_\mu^i\sigma^i - g'B_\mu\sigma^3) = \frac{i}{2}\begin{pmatrix} gW_\mu^3 - g'B_\mu & g(W_\mu^1 - iW_\mu^2) \\ g(W_\mu^1 + iW_\mu^2) & -gW_\mu^3 + g'B_\mu \end{pmatrix}$$

$$= \frac{i}{2}\begin{pmatrix} \sqrt{g^2 + g'^2}Z_\mu & g\sqrt{2}W_\mu^+ \\ g\sqrt{2}W_\mu^- & \sqrt{g^2 + g'^2}Z_\mu \end{pmatrix}$$

Where the relationship between the mass and gauge symmetry basis are as follows.

$$W_\mu^+ = \frac{1}{\sqrt{2}}(W_\mu^1 - iW_\mu^2) \tag{A.5}$$

$$W_\mu^- = \frac{1}{\sqrt{2}}(W_\mu^1 + iW_\mu^2) \tag{A.6}$$

$$Z_\mu = c_w W_\mu^3 - s_w B_\mu \tag{A.7}$$

$$A_\mu = s_w W_\mu^3 + c_w B_\mu \tag{A.8}$$

With $c_w = \dfrac{g}{\sqrt{g^2+g'^2}}$ and $s_w = \dfrac{g'}{\sqrt{g^2+g'^2}}$. Consider the expansion of the terms to be incldued in the Lagrangian.

$$V^\mu V_\nu = \frac{-1}{4}\begin{pmatrix} \sqrt{g^2+g'^2}Z^\mu & g\sqrt{2}W^{+\mu} \\ g\sqrt{2}W^{-\mu} & \sqrt{g^2+g'^2}Z^\mu \end{pmatrix}\begin{pmatrix} \sqrt{g^2+g'^2}Z_\nu & g\sqrt{2}W_\nu^+ \\ g\sqrt{2}W_\nu^- & \sqrt{g^2+g'^2}Z_\nu \end{pmatrix} \tag{A.9}$$

$$\mathrm{Tr}[V^\mu V_\nu] = \frac{-1}{2}((g^2+g'^2)Z^\mu Z_\nu + g^2 W^{+\mu}W_\nu^- + g^2 W^{-\mu}W_\nu^+) \tag{A.10}$$
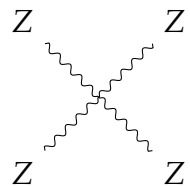
$$\mathrm{Tr}[V^\mu V_\nu]\mathrm{Tr}[V_\mu V^\nu] = \frac{(g^2+g'^2)^2}{4}(Z^\mu Z_\mu)^2 + g^2(g^2+g'^2)(Z^\mu Z^\nu W_\mu^- W_\nu^+) \tag{A.11}$$

$$+\frac{g^4}{2}(W^{-\mu}W_\mu^+)^2 + \frac{g^4}{2}(W^{-\mu}W^{+\nu}W_\mu^- W_\nu^+) \tag{A.12}$$
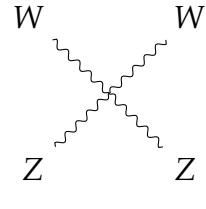
$$\mathrm{Tr}[V^\mu V_\mu]^2 = \frac{(g^2+g'^2)^2}{4}(Z^\mu Z_\mu)^2 + g^2(g^2+g'^2)(Z^\mu Z^\nu W_\mu^- W_\nu^+) \tag{A.13}$$

$$+g^4(W^{-\mu}W_\mu^+)^2 \tag{A.14}$$
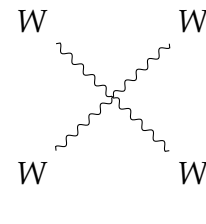
These two terms change the cross section for the vector boson scattering processes at CLIC that involve $ZZ \to ZZ$, $W^+W^- \to ZZ$, $ZZ \to W^+W^-$ and $W^+W^- \to W^+W^-$.

$$\subset (\alpha_4 + \alpha_5)\frac{(g^2+g'^2)^2}{4} \tag{A.15}$$

$$\subset (\alpha_4 + \alpha_5)g^2(g^2 + g'^2) \qquad\qquad (A.16)$$

$$\subset (\alpha_4 + 2\alpha_5)\frac{g^4}{2} \text{ and } \frac{g^4}{2}\alpha_4 \qquad\qquad (A.17)$$

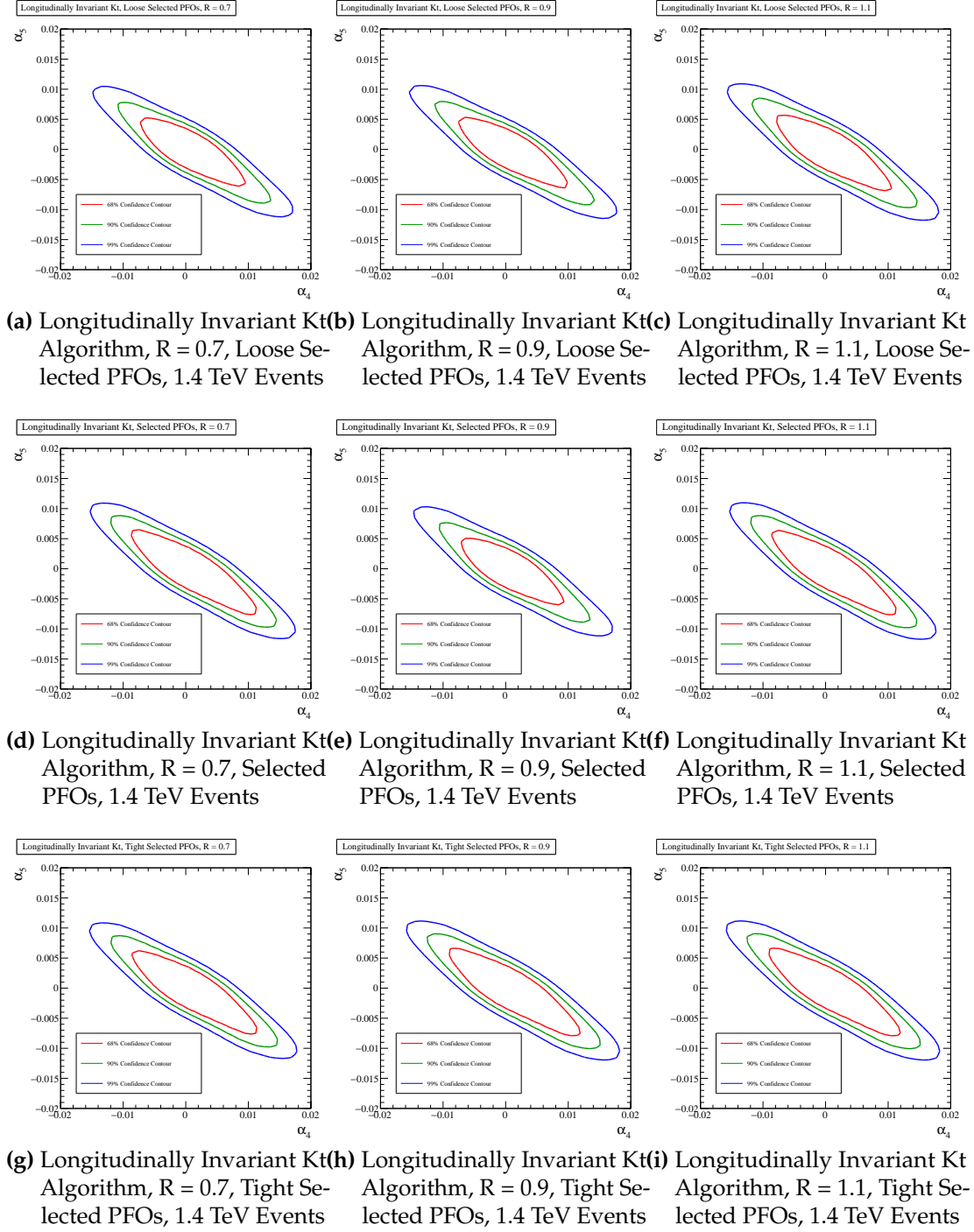## A.2. χ^2 Contour Plots for Jet Algorithm Optimisation

(a) Longitudinally Invariant Kt Algorithm, R = 0.7, Loose Selected PFOs, 1.4 TeV Events

(b) Longitudinally Invariant Kt Algorithm, R = 0.9, Loose Selected PFOs, 1.4 TeV Events

(c) Longitudinally Invariant Kt Algorithm, R = 1.1, Loose Selected PFOs, 1.4 TeV Events

(d) Longitudinally Invariant Kt Algorithm, R = 0.7, Selected PFOs, 1.4 TeV Events

(e) Longitudinally Invariant Kt Algorithm, R = 0.9, Selected PFOs, 1.4 TeV Events

(f) Longitudinally Invariant Kt Algorithm, R = 1.1, Selected PFOs, 1.4 TeV Events

(g) Longitudinally Invariant Kt Algorithm, R = 0.7, Tight Selected PFOs, 1.4 TeV Events

(h) Longitudinally Invariant Kt Algorithm, R = 0.9, Tight Selected PFOs, 1.4 TeV Events

(i) Longitudinally Invariant Kt Algorithm, R = 1.1, Tight Selected PFOs, 1.4 TeV Events

Figure A.1.: χ^2 Sensitivity contours for the qqqq$\nu\nu$ final state arising from a fit to $\cos\theta^*_{\text{Jets}}$ at 1.4 TeV for different values of jet reconstruction parameters.
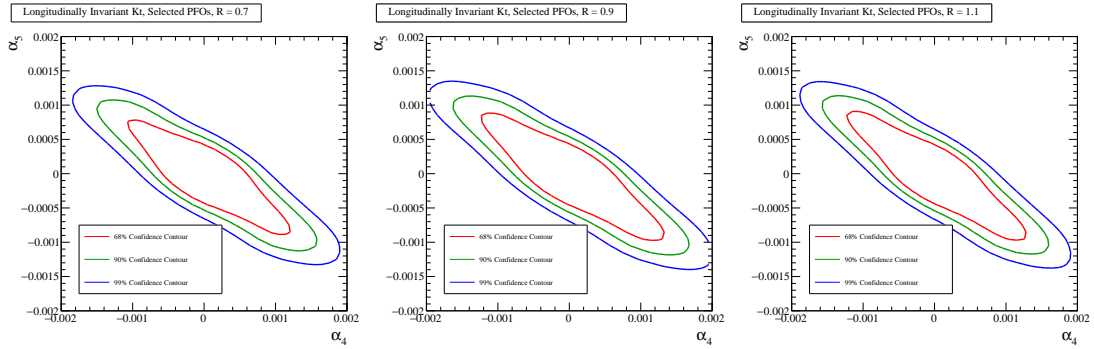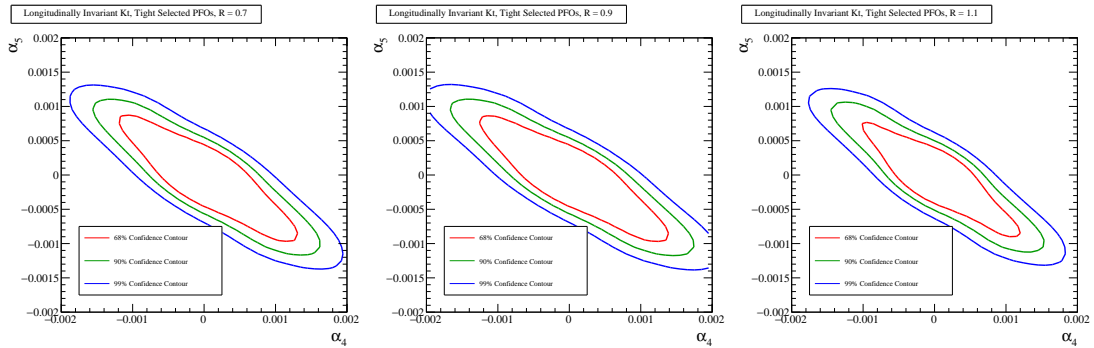
(a) Longitudinally Invariant Kt Algorithm, R = 0.7, Loose Selected PFOs, 1.4 TeV Events

(b) Longitudinally Invariant Kt Algorithm, R = 0.9, Loose Selected PFOs, 1.4 TeV Events

(c) Longitudinally Invariant Kt Algorithm, R = 1.1, Loose Selected PFOs, 1.4 TeV Events

(d) Longitudinally Invariant Kt Algorithm, R = 0.7, Selected PFOs, 1.4 TeV Events

(e) Longitudinally Invariant Kt Algorithm, R = 0.9, Selected PFOs, 1.4 TeV Events

(f) Longitudinally Invariant Kt Algorithm, R = 1.1, Selected PFOs, 1.4 TeV Events

(g) Longitudinally Invariant Kt Algorithm, R = 0.7, Tight Selected PFOs, 1.4 TeV Events

(h) Longitudinally Invariant Kt Algorithm, R = 0.9, Tight Selected PFOs, 1.4 TeV Events

(i) Longitudinally Invariant Kt Algorithm, R = 1.1, Tight Selected PFOs, 1.4 TeV Events

Figure A.2.: χ^2 as a function of α_4 assuming $\alpha_5 = 0$ for the qqqq$\nu\nu$ final state arising from a fit to $\cos\theta^*_{\text{Jets}}$ at 1.4 TeV for different values of jet reconstruction parameters.

(a) Longitudinally Invariant Kt Algorithm, R = 0.7, Loose Selected PFOs, 1.4 TeV Events **(b)** Longitudinally Invariant Kt Algorithm, R = 0.9, Loose Selected PFOs, 1.4 TeV Events **(c)** Longitudinally Invariant Kt Algorithm, R = 1.1, Loose Selected PFOs, 1.4 TeV Events

(d) Longitudinally Invariant Kt Algorithm, R = 0.7, Selected PFOs, 1.4 TeV Events **(e)** Longitudinally Invariant Kt Algorithm, R = 0.9, Selected PFOs, 1.4 TeV Events **(f)** Longitudinally Invariant Kt Algorithm, R = 1.1, Selected PFOs, 1.4 TeV Events

(g) Longitudinally Invariant Kt Algorithm, R = 0.7, Tight Selected PFOs, 1.4 TeV Events **(h)** Longitudinally Invariant Kt Algorithm, R = 0.9, Tight Selected PFOs, 1.4 TeV Events **(i)** Longitudinally Invariant Kt Algorithm, R = 1.1, Tight Selected PFOs, 1.4 TeV Events

Figure A.3.: χ^2 as a function of α_5 assuming $\alpha_4 = 0$ for the $qqqq\nu\nu$ final state arising from a fit to $\cos\theta^*_{\text{Jets}}$ at 1.4 TeV for different values of jet reconstruction parameters.

(a) Longitudinally Invariant Kt Algorithm, R = 0.7, Loose Selected PFOs, 3 TeV Events

(b) Longitudinally Invariant Kt Algorithm, R = 0.9, Loose Selected PFOs, 3 TeV Events

(c) Longitudinally Invariant Kt Algorithm, R = 1.1, Loose Selected PFOs, 3 TeV Events

(d) Longitudinally Invariant Kt Algorithm, R = 0.7, Selected PFOs, 3 TeV Events

(e) Longitudinally Invariant Kt Algorithm, R = 0.9, Selected PFOs, 3 TeV Events

(f) Longitudinally Invariant Kt Algorithm, R = 1.1, Selected PFOs, 3 TeV Events

(g) Longitudinally Invariant Kt Algorithm, R = 0.7, Tight Selected PFOs, 3 TeV Events

(h) Longitudinally Invariant Kt Algorithm, R = 0.9, Tight Selected PFOs, 3 TeV Events

(i) Longitudinally Invariant Kt Algorithm, R = 1.1, Tight Selected PFOs, 3 TeV Events

Colophon

This thesis was made in LaTeX 2$_\varepsilon$ using the "hepthesis" class [3].

Bibliography

[1] Toshinori Abe et al. The International Large Detector: Letter of Intent. 2010, 1006.3396.

[2] S. Agostinelli et al. GEANT4: A Simulation toolkit. *Nucl. Instrum. Meth.*, A506:250–303, 2003.

[3] Andy Buckley. The hepthesis LaTeX class.

[4] Matteo Cacciari, Gavin P. Salam, and Gregory Soyez. FastJet User Manual. *Eur. Phys. J.*, C72:1896, 2012, 1111.6097.

[5] F. Gaede. Marlin and LCCD: Software tools for the ILC. *Nucl. Instrum. Meth.*, A559:177–180, 2006.

[6] Andreas Hoecker, Peter Speckmayer, Joerg Stelzer, Jan Therhaag, Eckhard von Toerne, and Helge Voss. TMVA: Toolkit for Multivariate Data Analysis. *PoS*, ACAT:040, 2007, physics/0703039.

[7] Wolfgang Kilian, Thorsten Ohl, and Jurgen Reuter. WHIZARD: Simulating Multi-Particle Processes at LHC and ILC. *Eur. Phys. J.*, C71:1742, 2011, 0708.4233.

[8] Lucie Linssen, Akiya Miyamoto, Marcel Stanitzki, and Harry Weerts. Physics and Detectors at CLIC: CLIC Conceptual Design Report. 2012, 1202.5940.

[9] J. S. Marshall, A. MÃijnnich, and M. A. Thomson. Performance of Particle Flow Calorimetry at CLIC. *Nucl. Instrum. Meth.*, A700:153–162, 2013, 1209.4039.

[10] P. Mora de Freitas and H. Videau. Detector simulation with MOKKA / GEANT4: Present and future. In *Linear colliders. Proceedings, International Workshop on physics and experiments with future electron-positron linear colliders, LCWS 2002, Seogwipo, Jeju Island, Korea, August 26-30, 2002*, pages 623–627, 2002.

[11] Mauro Moretti, Thorsten Ohl, and Jurgen Reuter. O'Mega: An Optimizing matrix

element generator. 2001, hep-ph/0102195.

[12] André Sailer. *Radiation and Background Levels in a CLIC Detector due to Beam-Beam Effects*. PhD thesis, CERN, 2012-05-09.

[13] Taikan Suehara and Tomohiko Tanabe. LCFIPlus: A Framework for Jet Analysis in Linear Collider Studies. *Nucl. Instrum. Meth.*, A808:109–116, 2016, 1506.08371.

[14] M. A. Thomson. Particle Flow Calorimetry and the PandoraPFA Algorithm. *Nucl. Instrum. Meth.*, A611:25–40, 2009, 0907.3577.

List of figures

List of tables